INTERNATIONAL JOURNAL FOR NUMERICAL METHODS IN FLUIDS
Int. J. Numer. Meth. Fluids **30**: 831–843 (1999)

EXPLICIT FINITE VOLUME NON-OSCILLATORY SCHEMES FOR 2D TRANSIENT FREE-SURFACE FLOWS

MING-HSENG TSENG*

National Center for High-Performance Computing, 7 R&D Road VI, Science Based Research Park, PO Box 19-136, Hsinchu, Taiwan, Republic of China

SUMMARY

A class of high-resolution non-oscillatory shock-capturing Roe, TVD and ENO explicit schemes in finite volume approach are presented for the computation of 2D unsteady rapidly varied open channel flows. In order to apply these schemes to simulate the hydraulic phenomena in field, the Strang-type operator splitting technique is adopted to treat the flow with bottom slope and friction terms. Verifications of the proposed schemes are made by comparison with analytical solutions or experimental data, and very good agreements are obtained. To illustrate the efficiency and stability of the present algorithms, four typical problems of rapidly varied flows are solved and the results of different schemes are compared. It is demonstrated that the proposed method is accurate, robust and highly stable even in the flows with very strong discontinuites, which need no tuning of any adjustable parameter, such as artificial viscosity coefficient, as other methods do, and is a reliable mathematical modeling for 2D practical hydraulic engineering applications. Copyright © 1999 John Wiley & Sons, Ltd.

KEY WORDS: explicit high-resolution non-oscillatory shock-capturing scheme; finite volume; 2D unsteady rapidly varied open channel flows; operator splitting

1. INTRODUCTION

In recent years, several numerical schemes satisfying conservative, monotonicity preserving and shock-capturing properties for solving hyperbolic partial differential equations have appeared in the literature. The schemes are derived from the scalar wave equation, and generalization of these schemes to systems of equations are always accompanied by the technique known as approximate Riemann solvers. The approximate Riemann solvers include the Roe's flux difference splitting method [1], the Van Leer's flux vector splitting method [2], and the Osher scheme [3]. Extensive survey of the state-of-the-art of high-resolution shock-capturing schemes, same as total variation diminishing (TVD) and essentially non-oscillatory (ENO), for the gas dynamics equations has been given by Yee [4]. With the advances made in the computational techniques, the high-resolution shock-capturing schemes have been successfully applied to the computation of rapidly varied free-surface flows by many researchers [5–9].

* Correspondence to: National Center for High-Performance Computing, 7 R&D Road VI, Science Based Research Park, PO Box 19-136, ;Hsinchu;, Taiwan, Republic of China. Tel.: + 886 3 5776085, ext. 362; fax: + 886 3 5773538; e-mail: c00mht00@nchc.gov.tw

CCC 0271–2091/99/150831–13$17.50

Received March 1998
Revised August 1998

Jimenez and Chaudhry [10] used the MacCormack scheme with artificial viscosity to simulate 2D supercritical flow, Alcrudo and Navarro [11] introduced Godunov-type (MUSCL) scheme to 2D shallow water equations. Yang and Hsu [12] utilized Van Leer's flux vector splitting method to 2D unsteady bore wave diffraction. Zhao *et al.* [13] invoked the Osher scheme to 2D hydraulic shock wave modeling. Although such schemes reported good results near discontinuities, they may have needed tuning of the artificial viscosity coefficient case by case, neglected the source terms, or used a first-order scheme in their model.

In this paper, a finite volume approach based on high-resolution non-oscillatory schemes, including a first-order Roe scheme, second-order TVD and ENO schemes, and a third-order ENO scheme, are implemented for the discretization of the 2D shallow water equations. The schemes are using Harten's interpolations to achieve high-order-accurate (Harten [14], Harten and Osher [15] and Hsu [16]). The new features employ a flux difference splitting method instead of a flux vector splitting method, as in the previous research [12] for the Roe's approximate Riemann solver. For explicit time-accurate schemes, the Strang-type operator splitting technique [17] is utilized for computing the flow with source terms. The proposed model has been devised to perform integration on body-fitted meshes in an attempt to overcome the difficulty of having curved boundaries.

The contents of this paper are organized as follows. Mathematical formulation of 2D shallow water equations are described in Section 2. Numerical techniques and its characteristic properties are illuminated in Section 3. In Section 4, several 2D steady and unsteady rapidly varied open channel flows with surges computations are given to validate and demonstrate the accurate, robust and highly stable features of the current schemes. Finally, concluding remarks are given in the last section.

2. MATHEMATICAL FORMULATION

Under the assumption of a homogeneous, incompressible, viscous flow characterized by a hydrostatic pressure distribution, with wind, Coriolis forces and horizontal internal shear stresses neglected, the depth-integrated equations of motion form the fundamental equations for 2D transient free-surface flows.

2D unsteady shallow water equations, also referred to as the St. Venant equations, in terms of flow variables $\mathbf{Q} = (h, hu, hv)^T$, may be expressed in conservation law form as

$$\frac{\partial \mathbf{Q}}{\partial t} + \nabla \mathbf{F} = \frac{\partial \mathbf{Q}}{\partial t} + \frac{\partial \mathbf{E}}{\partial x} + \frac{\partial \mathbf{G}}{\partial y} = \mathbf{S}, \tag{1}$$

since $\mathbf{F} = i\mathbf{E} + j\mathbf{G}$, where

$$\mathbf{E} = \begin{pmatrix} hu \\ hu^2 + \frac{1}{2}gh^2 \\ huv \end{pmatrix}, \qquad \mathbf{G} = \begin{pmatrix} hv \\ huv \\ hv^2 + \frac{1}{2}gh^2 \end{pmatrix}, \qquad \mathbf{S} = \begin{pmatrix} 0 \\ gh\left(S_{0_x} - \dfrac{n^2 u\sqrt{u^2+v^2}}{h^{4/3}}\right) \\ gh\left(S_{0_y} - \dfrac{n^2 v\sqrt{u^2+v^2}}{h^{4/3}}\right) \end{pmatrix}. \tag{2}$$

Here, h is the water depth, u and v are velocity components in the x- and y-direction respectively, g is the gravitational constant, S_{0_x} and S_{0_y} are channel bottom slopes in the x- and y-direction respectively, and n is the Manning roughness coefficient.

3. NUMERICAL METHODS

3.1. Finite volume approach

The system represented by Equation (1) is integrated by a finite volume technique on each of the cells covering the whole domain, by invoking the mean value theorem and the divergence theorem, given as

$$\frac{\partial \bar{\mathbf{Q}}}{\partial t} = -\frac{1}{V}\oint_s n\cdot\mathbf{F}\,\mathrm{d}s + \bar{\mathbf{S}}, \tag{3}$$

where $\bar{\mathbf{Q}}$ and $\bar{\mathbf{S}}$ stand for a mean quantity referred to the center of the volume V and n is the normal vector of the volume surface s.

Equation (3) can be discretized now provided that the surface integral is approximated by a sum over the four sides of a numerical flux in the following way (with the overbar omitted for brevity)

$$\frac{\partial \mathbf{Q}}{\partial t} = -\frac{1}{V}\sum_{k=1}^{4}(n\cdot\mathbf{F}s)_k + \mathbf{S}. \tag{4}$$

Following the technique proposed by Roe for constructing a suitable coefficient matrix to define a modified linear but equivalent system of conservation laws (Alcrudo and Navarro [11]), an approximate Jacobian, $\mathbf{A}$, of the normal flux with real eigenvalues a^ℓ of the form can be found

$$a^1 = un_x + vn_y, \qquad a^2 = un_x + vn_y + c, \qquad a^3 = un_x + vn_y - c, \tag{5}$$

where $c = \sqrt{gh}$ is the wave celerity. The corresponding right and left eigenvector matrices for $\mathbf{A}$ are

$$\mathbf{R} = \frac{1}{2c}\begin{pmatrix} 0 & 1 & 1 \\ -2cn_y & u+cn_x & u-cn_x \\ 2cn_x & v+cn_y & v-cn_y \end{pmatrix}, \qquad \mathbf{L} = \begin{pmatrix} un_y - vn_x & -n_y & n_x \\ c - un_x - vn_y & n_x & n_y \\ c + un_x + vn_y & -n_x & -n_y \end{pmatrix}. \tag{6}$$

Due to the hyperbolicity, we have

$$\mathbf{A} = \mathbf{R}\Lambda\mathbf{L}, \quad \Lambda = \mathrm{diag}\{a^\ell\}. \tag{7}$$

3.2. High-resolution non-oscillatory schemes

A conservative scheme for Equation (4) (with the source terms omitted temporarily) can be written as

$$\mathbf{Q}_{i,j}^{m+1} = \mathbf{Q}_{i,j}^{m} - \frac{\Delta t}{V}\left[\sum_{k=-1/2}^{1/2}(n\cdot\mathbf{F}s)_{i+k,j}^{m} + \sum_{k=-1/2}^{1/2}(n\cdot\mathbf{F}s)_{i,j+k}^{m}\right] = \mathscr{L}(\Delta t)\mathbf{Q}_{i,j}^{m}, \tag{8}$$

where $(n\cdot\mathbf{F}s)_{i+k,j}$ and $(n\cdot\mathbf{F}s)_{i,j+k}$ are the so-called (modified) numerical fluxes.

The first-order Roe scheme and high-order schemes, including second-order TVD and ENO schemes and a third-order ENO scheme, can be applied to the finite volume approach for Equation (8).

The numerical flux of these high-resolution non-oscillatory schemes in Equation (8) is defined by

$$(n\cdot\mathbf{F}s)_{i+1/2,j}=\frac{1}{2}[(n\cdot\mathbf{F}s)_{i,j}+(n\cdot\mathbf{F}s)_{i+1,j}+\mathbf{R}_{i+1/2,j}\mathbf{\Phi}_{i+1/2,j}s_{i+1/2,j}]. \tag{9}$$

The components of $\mathbf{\Phi}_{i+1/2,j}$ are defined as

$$\begin{aligned}\phi^l_{i+1/2,j}=&\epsilon\sigma(a^l_{i+1/2,j})(g^l_{i,j}+g^l_{i+1,j})+\theta\bar{\sigma}(a^l_{i+1/2,j})(d^l_{i,j}+d^l_{i+1,j})\\&-\psi(a^l_{i+1/2,j}+c\gamma^l_{i+1/2,j}+\theta\delta^l_{i+1/2,j})\alpha^l_{i+1/2,j},\end{aligned} \tag{10}$$

where $\alpha^l_{i+1/2,j}$, called the characteristic variables, are defined as

$$\boldsymbol{\alpha}_{i+1/2,j}=\mathbf{L}_{i+1/2,j}(\mathbf{Q}_{i+1,j}-\mathbf{Q}_{i,j}), \tag{11}$$

and other high-order terms are given by

$$\sigma(z)=\frac{1}{2}[\psi(z)-\lambda z^2], \tag{12}$$

$$\bar{\sigma}(z)=\begin{cases}(\lambda^2|z|^3-3\lambda|z|^2+2|z|)/6, & \text{if } |\alpha^l_{i-1/2,j}|\le|\alpha^l_{i+1/2,j}|\\(\lambda^2|z|^3-|z|)/6, & \text{otherwise.}\end{cases}, \tag{13}$$

and

$$g^l_{i,j}=m(\alpha^l_{i+1/2,j}-\beta\bar{m}(\Delta_-\alpha^l_{i+1/2,j},\Delta_+\alpha^l_{i+1/2,j}),\alpha^l_{i-1/2,j}+\beta\bar{m}(\Delta_-\alpha^l_{i-1/2,j},\Delta_+\alpha^l_{i-1/2,j})), \tag{14}$$

$$d^l_{i,j}=\begin{cases}\bar{m}(\Delta_-\alpha^l_{i-1/2,j},\Delta_+\alpha^l_{i-1/2,j}), & \text{if } |\alpha^l_{i-1/2,j}|\le|\alpha^l_{i+1/2,j}|\\\bar{m}(\Delta_-\alpha^l_{i+1/2,j},\Delta_+\alpha^l_{i+1/2,j}), & \text{otherwise}\end{cases}, \tag{15}$$

$$\gamma^l_{i+1/2,j}=\begin{cases}\sigma(a^l_{i+1/2,j})(g^l_{i+1,j}-g^l_{i,j})/\alpha^l_{i+1/2,j}, & \text{if } \alpha^l_{i+1/2,j}\neq 0\\0 & \text{otherwise}\end{cases}, \tag{16}$$

$$\delta^l_{i+1/2,j}=\begin{cases}\bar{\sigma}(a^l_{i+1/2,j})(d^l_{i+1,j}-d^l_{i,j})/\alpha^l_{i+1/2,j}, & \text{if } \alpha^l_{i+1/2,j}\neq 0\\0 & \text{otherwise}\end{cases}, \tag{17}$$

and the limiter functions m, $\bar{m}$ and the entropy fix function ψ are defined as

$$m(a,b)=\begin{cases}s\ \min(|a|,|b|), & \text{if sign } a=\text{sign } b=s;\\0 & \text{otherwise}\end{cases}, \tag{18}$$

$$\bar{m}(a,b)=\begin{cases}a & \text{if } |a|\le|b|;\\b & \text{otherwise}\end{cases}, \tag{19}$$

$$\psi(z)=\begin{cases}|z|, & \text{if } |z|\ge\epsilon;\\(z^2+\epsilon^2)/2\epsilon, & \text{if } |z|<\epsilon\end{cases}, \tag{20}$$

where ϵ is a small positive number.

In the above equations, three free parameters ϵ, θ and β be used to let the first-order Roe scheme (ROE1), the second-order TVD scheme (TVD2), the second-order ENO scheme (ENO2) and the third-order ENO scheme (ENO3) to be expressed in the same formulations. The relations are

$$\begin{array}{llll} \epsilon = 0 & \theta = 0 & \beta = 0 & \rightarrow \text{Roe1} \\ \epsilon = 1 & \theta = 0 & \beta = 0 & \rightarrow \text{TVD2} \\ \epsilon = 1 & \theta = 0 & \beta = 0.5 & \rightarrow \text{ENO2} \\ \epsilon = 1 & \theta = 1 & \beta = 0 & \rightarrow \text{ENO3} \end{array} \tag{21}$$

The subscript $(i+1/2, j)$ denotes the intermediate state between grid points (i, j) and $(i+1, j)$, and can be defined following Roe [1] as

$$\begin{aligned} u_{i+1/2,j} &= \frac{\sqrt{h_{i,j}}\,u_{i,j} + \sqrt{h_{i+1,j}}\,u_{i+1,j}}{\sqrt{h_{i,j}} + \sqrt{h_{i+1,j}}}, \\ v_{i+1/2,j} &= \frac{\sqrt{h_{i,j}}\,v_{i,j} + \sqrt{h_{i+1,j}}\,v_{i+1,j}}{\sqrt{h_{i,j}} + \sqrt{h_{i+1,j}}}, \\ c_{i+1/2,j} &= \sqrt{g(h_{i,j} + h_{i+1,j})/2}. \end{aligned} \tag{22}$$

For Equation (4) with non-zero source terms, Strang-type operator splitting technique [17] was employed and the complete integrating schemes can be expressed as

$$\mathbf{Q}^{m+1} = \mathscr{L}_S(\Delta t/2)\mathscr{L}(\Delta t)\mathscr{L}_S(\Delta t/2)\mathbf{Q}^m, \tag{23}$$

where the operator $\mathscr{L}$ is defined previously in Equation (8) and the operator $\mathscr{L}_S$ for the source terms is given by

$$\mathscr{L}_S(\Delta t)\mathbf{Q}^m = \mathbf{Q}_m + \Delta t S^m + \frac{\Delta t^2}{2}\left(\frac{\partial \mathbf{S}}{\partial \mathbf{Q}}\right)^m \mathbf{S}^m. \tag{24}$$

3.3. Numerical stability

By numerical stability requirement, the time step Δt must be selected based on the Courant–Friedrich–Lewy stability criterion. The maximum allowable time step is limited in this paper by the following

$$\Delta t \leq \text{CFL}\left[\frac{V}{|u_i s_i| + cs}\right], \tag{25}$$

where $0 < \text{CFL} \leq 1$ is the Courant number. The above defined schemes are stable for a CFL number almost equal to 1.

3.4. Boundary and initial conditions

The above described schemes are for the interior points. For subcritical flows, two external conditions must be specified at the inflow boundary, whereas only one is required at the outflow boundary and the remaining unknown variables are furnished by the Riemann invariants. Supercritical flows required the imposition of three inflow boundary conditions and none at the downstream side. And the boundary condition imposed on the solid wall is a no-flux condition.

The information required to start the time evolution computation on the 2D domain has been provided by specifying the values of the three independent variables (h, u, v) at every cell (i, j) for time $t = 0$, and assuming them to be uniform over the cell represented by that point.

4. RESULTS AND DISCUSSION

In this section, the numerical results are exhibited that were obtained for several test problems used to validate and illustrate the efficiency and stability of the proposed algorithms, and the results of different schemes are compared.

Computations for the problems included herein were done on a Pentium-100 PC equipped with a 16 magebyte RAM.

4.1. 1D dam-break

The first situation is supposed to simulate the catastrophic flood following the collapse of a dam, although the dam-break flow in a horizontal frictionless rectangular channel is not a real world state, it serves as an ideal validation for numerical simulation, as analytical solution only exists in such simplified case. The problem is briefly described as follows. Two different depths of water, termed as reservoir depth (H_r) and tailwater depth (H_t) respectively, in a 1 km long channel are separated by a dam located at the middle of the channel. Initially the dam is instantaneously and completely collapsed, and numerical solutions are carried out to simulate the ensuing wave propagation process. The depth ratio (H_r/H_t) is used to defined a dam-break problem. When the depth ratio is less than 2, the flow remains subcritical. For depth more than 2, the flow downstream of the dam location changes to supercritical while the flow in the reservoir portion still remains subcritical. This change in the flow condition is largely responsible for the problems encountered in simulating the dam-break problem. The severity of a problem increases as the depth ratio increases.

The grid size is 10 m in x space, and the CFL number is set to unity for all of the schemes. The resulting water surface and velocity profiles along the channel, for $H_r/H_t = 1000$ case at time $t = 30$ s after dam failure, computed by the ROE1, TVD2, ENO2 and ENO3 schemes and the analytical solution are all shown in Figure 1(a) and (b) respectively. The computed results and the analytical solution are compared with quite satisfactory agreements, except for the ROE1 scheme, which is a first-order scheme and it has excessive numerical damping, and leads to a strong smearing of the discontinuities and an unphysical stationary jump appears at the dam location that spoils the solution. The quantitative comparison of relative error in L2 norm between the computed results and analytical solutions are shown in Table I, where the L2 norm is defined as $\sqrt{\Sigma_{i=1}^{n}(Y_{\text{computed},i} - Y_{\text{analytical},i})^2 / \Sigma_{i=1}^{n}(Y_{\text{analytical},i})^2}$. These results indicate that the ENO3, ENO2 and TVD2 scheme have notably better than that of the ROE1 scheme. The CPU time required is 1 s for the ENO2 scheme, and the computer time is almost equally among the ROE1, TVD2, ENO2 and ENO3 schemes.

4.2. Breaking of a circular dam

Another interesting test case for the analysis of the proposed algorithms performance is that of the breaking of a circular dam and the time evolution of the subsequent waves, same condition and geometry as Alcrudo and Navarro [11]. The high symmetry of the problem renders it an adequate example to prove the present schemes.

A cylindrical grid system was used, consisting of 50 cells following the tangential direction versus 25 cells of 1 m length along the radial direction. Two regions of still water separated by a cylindrical wall (radius = 11 m) and the depth ratio is set to 10, with 10 m water elevation on the inner side for the initial conditions.

Figure 2(a)–(d) illustrate the contours of water depth for the ROE1, TVD2, ENO2 and ENO3 schemes respectively, 0.69 s after dam failure. Computations were performed with a

CFL number of 1.0 for all of the schemes. The CPU time required is 6 s for the ENO2 scheme, and the ratio of the computer time among the ROE1, TVD2, ENO2 and ENO3 schemes is almost 0.67:1:1:1.

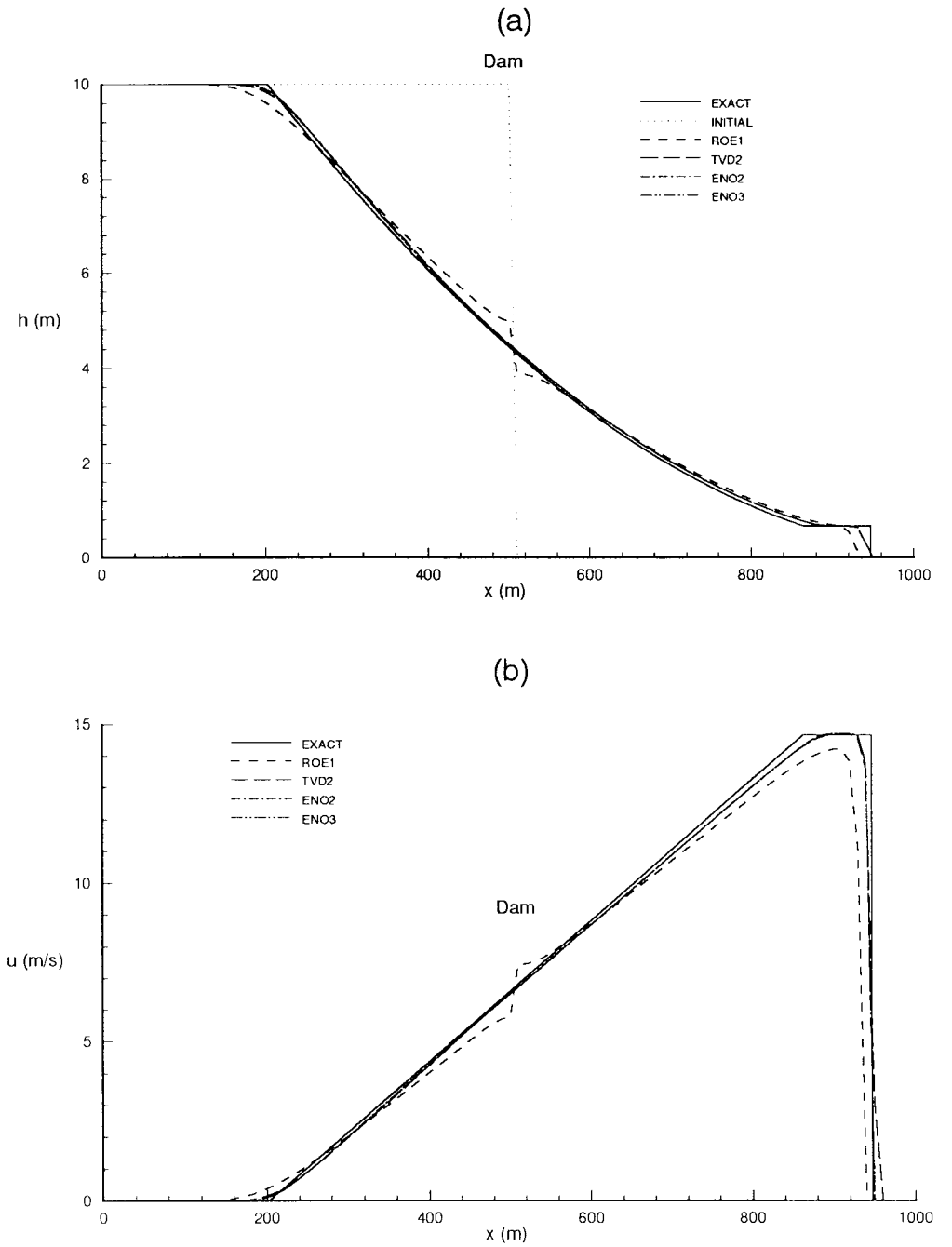

Figure 1. Profiles for 1D dam-break: (a) water surface; (b) velocity.

Table I. L2 norm for 1D dam-break

Scheme	L2 of depth (h)	L2 of velocity (u)
ROE1	0.044	0.311
TVD2	0.026	0.214
ENO2	0.025	0.238
ENO3	0.025	0.240

The results produced a perfect circular symmetry flow behavior as expected, and agreed very well with those of Alcrudo and Navarro [11]. In this sense, the finite volume formulation employed in this paper shows an advantage over classical finite difference methods. For a

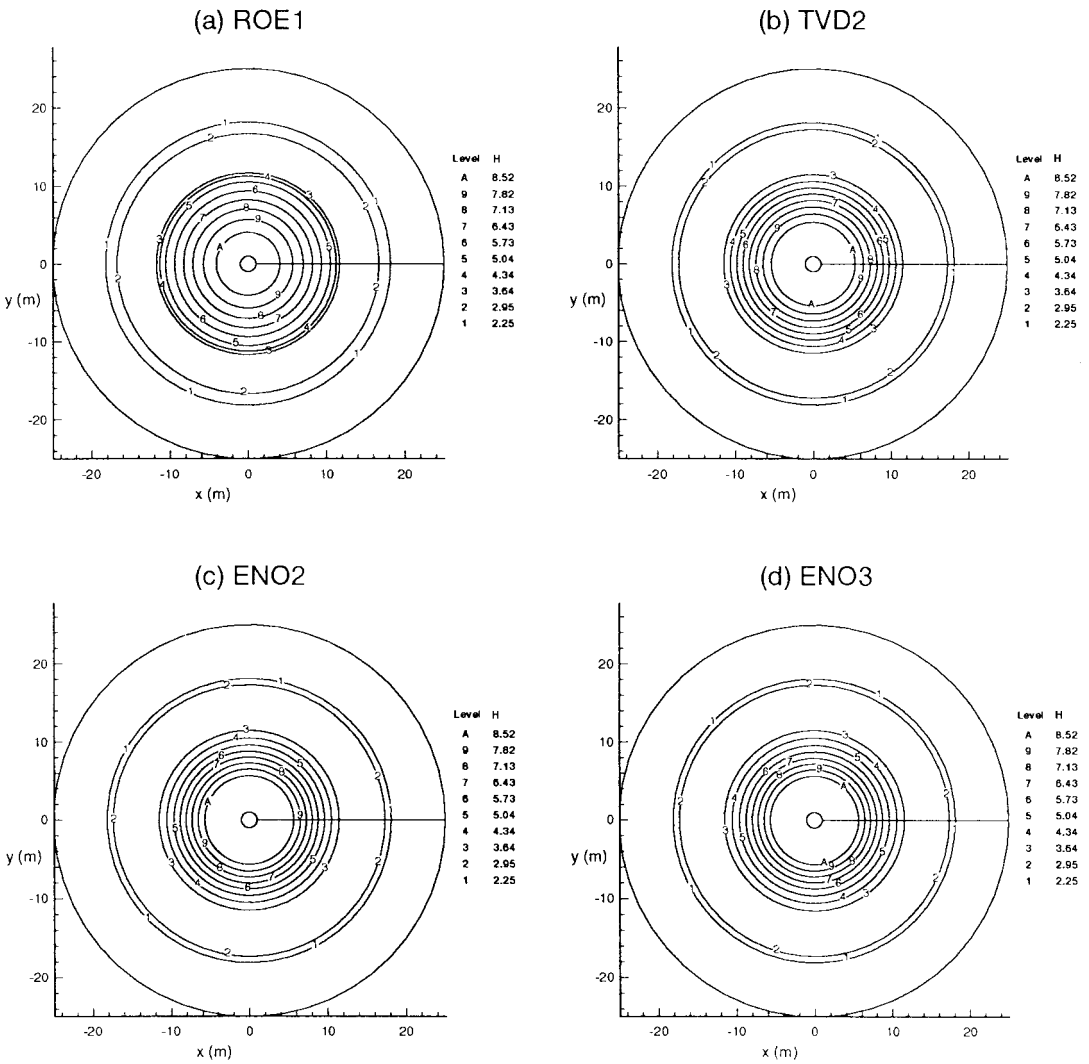

Figure 2. Depth contours for breaking of a circular dam.

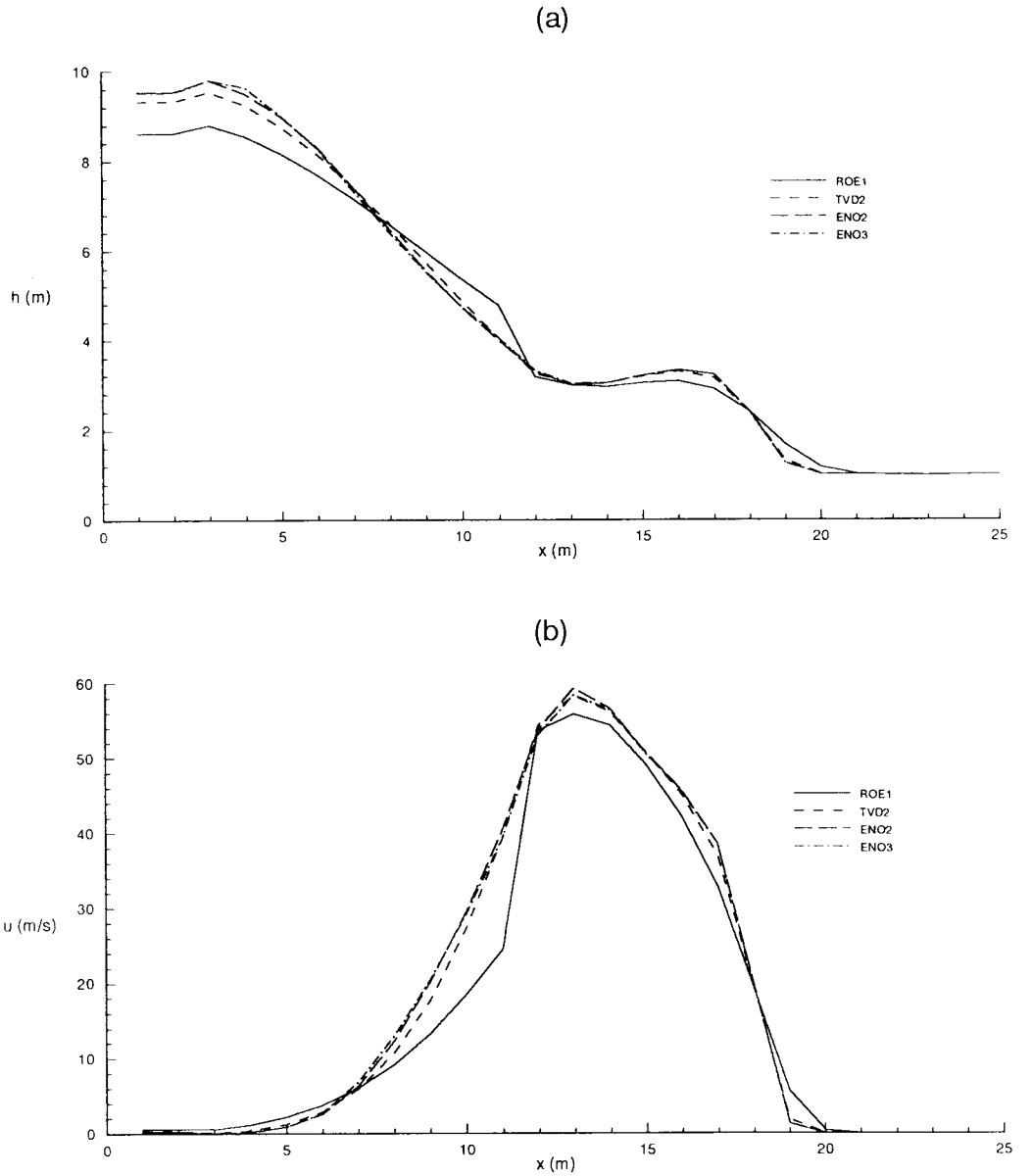

Figure 3. Comparison of radial profiles: (a) water surface; (b) velocity.

quantitative comparison of ROE1, TVD2, ENO2 and ENO3 schemes, computed results are shown in Figure 3(a) and (b). Figure 3(a) shows the comparison of computed radial water surface profile and Figure 3(b) represents the respective velocity plot. It is clear from these comparisons that TVD2, ENO2 and ENO3 schemes give similar results, since the ROE1 scheme has only a first-order accuracy, significant differences are exhibited with the other three schemes.

Table II. L2 norm for oblique hydraulic jump

Scheme	L2 of depth (h)	L2 of velocity (V)	L2 of angle (β)
ROE1	0.049	0.009	0.033
TVD2	0.036	0.007	0.006
ENO2	0.034	0.007	0.005
ENO3	0.033	0.007	0.004

4.3. Oblique hydraulic jump

The oblique hydraulic jump is induced by means of an interaction between a supercritical flow and a converging wall deflected through an angle θ. The shock wave is formed with an angle of β. As usual, this problem is used to test the scheme's ability to simulate the formation of a shock wave in 2D steady supercritical flow.

A 40×30 non-rectangular cell was utilized to reproduce the discontinuous flow in a non-prismatic channel, where $\theta = 8.95°$ for the converging side. The initial conditions were a

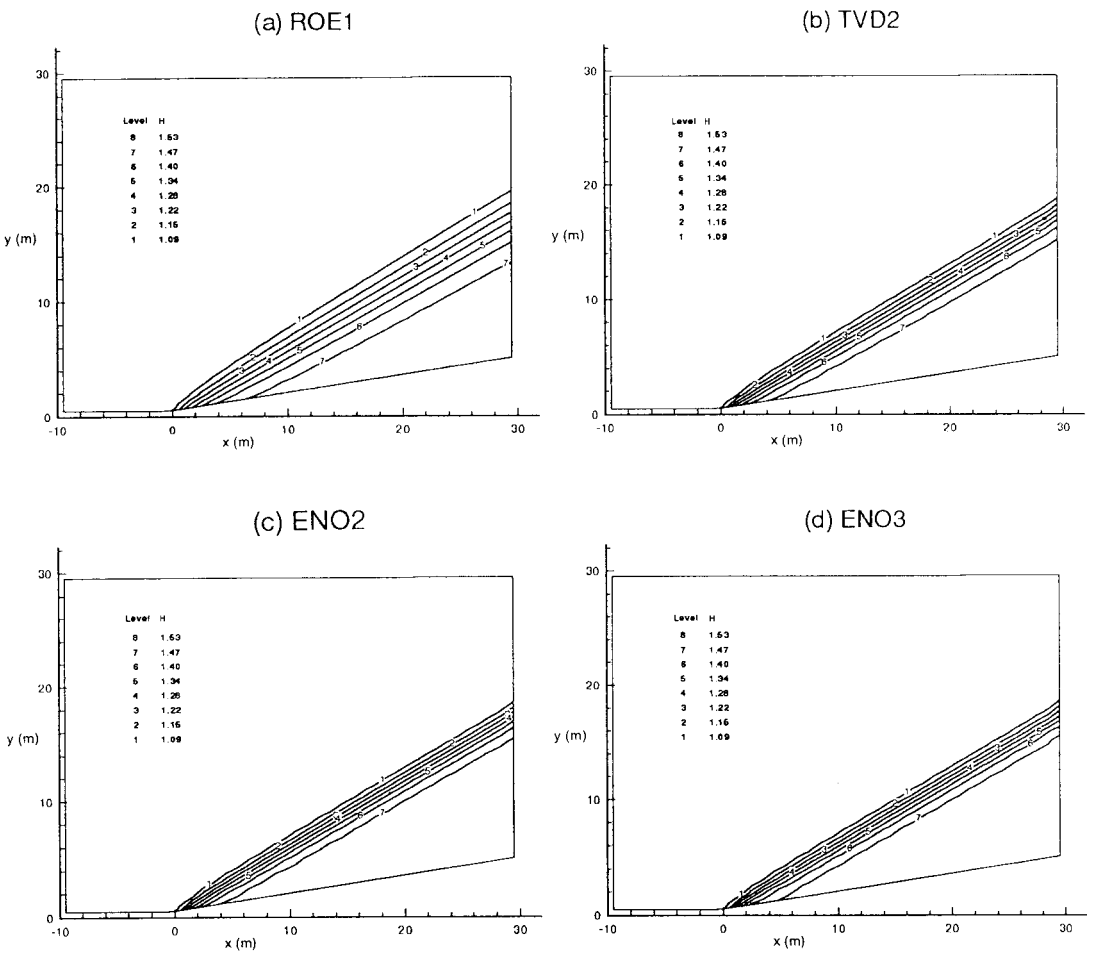

Figure 4. Depth contours for oblique hydraulic jump.

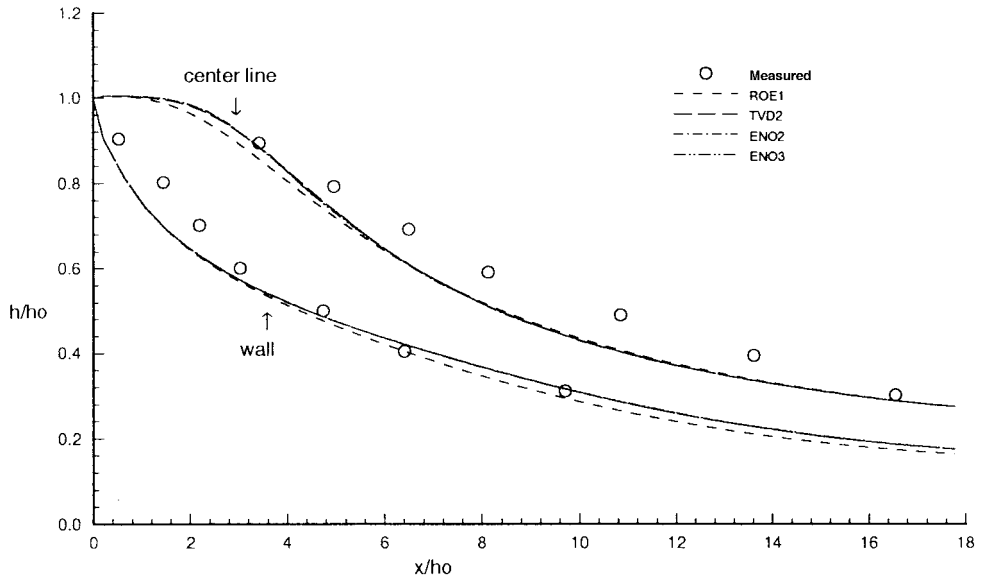

Figure 5. Water surface profiles at wall and centerline in a gradual expansion.

uniform water depth of 1 m, a flow velocity u of 8.57 m s^{-1} and $v = 0$, corresponding to a Froude number of 2.74. The supercritical flow boundary conditions were applied at the upstream side.

Using the described schemes, the computation converged to the steady state from the given initial and boundary conditions, that the CFL number is set to 0.9 for all of the schemes. The results are listed in Table II and the contours of water depth computed by the ROE1, TVD2, ENO2 and ENO3 schemes are plotted in Figure 4(a)–(d) respectively.

As can be verified from the above results, the agreements of the TVD2, ENO2 and ENO3 schemes with the analytical solution were very good and a discontinuous water surface devoid of oscillations was obtained. In the same manner as for the dam-break problem, the ROE1 scheme gives excessive numerical damping near the shock front. The CPU time required is 25 s for the ENO2 scheme, and the ratio of the computer time among the ROE1, TVD2, ENO2 and ENO3 schemes is almost 0.72:0.96:1:1.16.

4.4. Supercritical flow in a gradual expansion

Rouse *et al.* [18] suggested the following equation for a supercritical flow in a gradual expansion:

$$\frac{b_x}{b_0} = 0.5\left(\frac{x}{b_0 Fr_0}\right)^{1.5} + 0.5. \tag{26}$$

Here b_0 is the upstream channel width and b_x is the channel width at x location. The effect of source terms are considered. A Manning $n = 0.015$ is assumed and the bottom slope is zero.

The upstream Froude number is $Fr_0 = 2.0$ and $h_0/b_0 = 0.25$ with $b_0 = 1$. Due to symmetry, only half channel width is computed. The computed range is from $x/h_0 = 0$–18 and 43×21 cells are used. Computations were finished with a CFL number setting to 1 for all of the schemes. The CPU time required is 177 s for the ENO2 scheme, and the ratio of the computer time among the ROE1, TVD2, ENO2 and ENO3 schemes is almost 0.74:0.95:1:1.12.

Table III. L2 norm for supercritical flow in a gradual expansion

Scheme	L2 of depth (h)
ROE1	0.098
TVD2	0.095
ENO2	0.095
ENO3	0.096

Figure 5 shows the wall and centerline water surface profiles simulated by the ROE1, TVD2, ENO2 and ENO3 schemes together with the experimental data of Rouse *et al.* [18]. The computed results for the four schemes are similar to those of Jimenez and Chaudhry [10] and compare satisfactorily with the measured results. The quantitative comparison of relative error in L2 norm between the computed results and measured data are shown in Table III. These results indicate that the ENO3, ENO2 and TVD2 schemes seem to be slightly better than that of the ROE1 scheme.

5. CONCLUDING REMARKS

High-resolution non-oscillatory shock-capturing explicit schemes, including a first-order Roe scheme, second-order TVD and ENO schemes, and a third-order ENO scheme, in a finite volume approach are proposed for the computation of 2D transient free-surface flows involving hydraulic jumps and bores.

Verifications of all of the described schemes are made by comparison with analytical solutions or experimental data, and very good agreements are found, except for the ROE1 scheme which is a first-order scheme and it has excessive numerical damping and leads to a strong smearing of the discontinuities.

Based on solving the 1D dam-break problem, the breaking of a circular dam problem, the oblique hydraulic jump problem and the supercritical flow in a gradual expansion problem, it can be concluded that the results of the TVD2, ENO2 and ENO3 schemes perform almost equally well for such flow conditions, but comparable differences in accuracy are exhibited between the ROE1 scheme and the other three schemes. For cases without bottom slope and friction terms, the results indicate that the ENO3, ENO2 and TVD2 schemes are notably better than that of the ROE1 scheme. When considering the source terms effect, differences in accuracy are not so significant among the four schemes. Relatively speaking, however, the ENO3 scheme is the most accurate, the ENO2 scheme ranks second and the ROE1 scheme is the least accurate. On the other hand, the ROE1 scheme required the least computer time, while the ENO3 needed the most computer time. The numerical stability among the four schemes is identical and all the schemes are stable for a CFL number almost equal to 1.

It was demonstrated that the proposed method is accurate, robust and highly stable even in the flows with very strong discontinuites, which need no tuning of any adjustable parameter, such as artificial viscosity coefficient, as other methods do, and is a reliable mathematical modeling to solve 2D hydraulic shock wave problems.

For all practical purposes, the second-order ENO and TVD schemes based on Harten's ENO interpolations are preferred for practical applications in hydraulic engineering when computation time, overall accuracy and applicability are considered.

ACKNOWLEDGMENTS

The computer facilities and office provided for this study by the National Center for High-Performance Computing (NCHC) are hereby gratefully acknowledged. A portion of this work was supported by the National Science Council, Taiwan, under Grant No. NSC-86-2621-E-002-014 and is greatly appreciated. Thanks are also extended to Dr C.A. Hsu for providing many helpful discussions.

REFERENCES

1. P.L. Roe, 'Approximate Riemann solvers, parameter vectors, and difference schemes', *J. Comput. Phys.*, **43**, 357–372 (1981).
2. B. Van Leer, 'Flux-vector splitting for the Euler equations', in E. Krause (ed.), *Proc. 8th Int. Conf. on Numerical Methods in Fluid Dynamics*, Springer, Berlin, 1982, pp. 507–512.
3. S. Osher and F. Solomone, 'Upwind difference schemes for hyperbolic system of conservation laws', *Math. Comput.*, **38**, 339–374 (1982).
4. H.C. Yee, 'A class of high-resolution explicit and implicit shock-capturing methods', *NASA TM-101088*, 1989.
5. P. Glaister, 'Approximate Riemann solutions of the shallow water equations', *J. Hydraul. Res.*, **26**, 293–306 (1988).
6. F. Alcrudo, P. Garcia-Navarro and J.M. Saviron, 'Flux difference splitting for 1D open channel flow equations', *Int. J. Numer. Methods Fluids*, **14**, 1009–1018 (1992).
7. J.Y. Yang, C.A. Hsu and C.H. Chang, 'Computation of free surface flows, Part 1. One-dimensional dam-break flow', *J. Hydraul. Res.*, **31**, 19–34 (1993).
8. Lj. Savic and Jr.F.M. Holly, 'Dam-break flood waves computed by modified Godunov method', *J. Hydraul. Res.*, **31**, 187–204 (1993).
9. M. Nujic, 'Efficient implementation of non-oscillatory schemes for the computation of free-surface flows', *J. Hydraul. Res.*, **33**, 101–111 (1995).
10. O.F. Jimenez and M.H. Chaudhry, 'Computation of supercritical free-surface flows', *J. Hydraul. Eng. ASCE*, **114**, 377–395 (1988).
11. F. Alcrudo and P. Garcia-Navarro, 'A high-resolution Godunov-type scheme in finite volumes for the 2D shallow water equations', *Int. J. Numer. Methods Fluids*, **16**, 489–505 (1993).
12. J.Y. Yang and C.A. Hsu, 'Computation of free-surface flows, Part 2. Two-dimensional unsteady bore diffraction', *J. Hydraul. Res.*, **31**, 403–414 (1993).
13. D.H. Zhao, H.W. Shen, J.S. Lai and G.Q. Tabios III, 'Approximate Riemann solvers in FVM for 2D hydraulic shock wave modeling', *J. Hydraul. Eng. ASCE*, **122**, 863–883 (1996).
14. A. Harten, 'High resolution schemes for hyperbolic conservation laws', *J. Comput. Phys.*, **49**, 357–393 (1983).
15. A. Harten and S. Osher, 'Uniformly high-order-accurate non-oscillatory schemes. I', *SIAM J. Numer. Anal.*, **24**, 279–309 (1987).
16. C.A. Hsu, 'High-resolution non-oscillatory schemes for hyperbolic conservation laws with applications to aerodynamics', *Ph.D. Dissertation*, Institute of Applied Mechanics, Taiwan University, 1993.
17. G. Strang, 'On the construction and comparison of difference schemes', *SIAM J. Numer. Anal.*, **5**, 506–517 (1968).
18. H. Rouse, B.V. Bhoota and E.Y. Hsu, 'Design of channel expansions', *Trans. ASCE*, **116**, 347–363 (1951).

